Thermoplasmonic Membrane-Based Infrared Detector

Fei Yi, Hai Zhu, Jason C. Reed, Alexander Y. Zhu, and Ertugrul Cubukcu, *Member, IEEE*

***Abstract*— In this letter, we experimentally demonstrate, by integrating plasmonic nanoantennas, that membrane-based micromechanical resonators can become infrared (IR) active. The photo-thermomechanical effect induced by nanoantennas enables actuation of mechanical structures. Using this hybrid nanoantenna coupled mechanical device as a thermal IR detector, we achieved a current responsivity of 12 mA/W corresponding to a displacement responsivity of 98.7 μm/W and a thermal time constant of 5.7 ms at a wavelength of 6 μm. This approach can be extended to any mechanical resonator for new optomechanical sensing modalities.**

***Index Terms*— Nanoantenna, plasmonic absorber, nanomechanical resonator, infrared, thermal detector.**

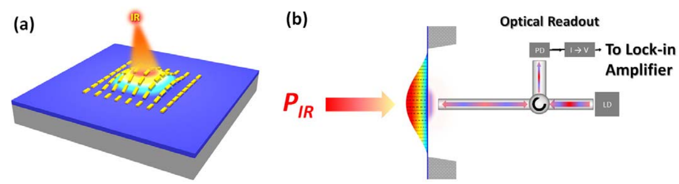

Fig. 1. (Color online) A schematic overview of the membrane based plasmomechanical infrared detector: (a) a plasmonic antenna absorber is formed by fabricating gold nanorod antennas on a commercial silicon nitride membrane. (b) The membrane also acts as one of the two reflectors of a fiber optic interferometer. The optical readout is formed by a 1550 nm laser (LD), a photodetector (PD), a current to voltage converter (I→V) and a lock-in amplifier. The infrared power, PIR, is supplied by a 6 μm laser.

I. Introduction

LOCALIZED surface plasmon modes, originating from the collective oscillations of the electron plasma in a metal nanostructure [1]–[4], have been explored for various applications ranging from biosensors to near-field optical microscopes and devices [5]–[8]. When excited resonantly, these modes can localize the freely propagating radiation and produce very high optical near field intensities while dissipating electromagnetic energy efficiently as heat due to high optical absorption in metals. This high optical absorption has led to the demonstration of absorbers for radiation from THz frequencies to the visible region [9]–[22]. Thermoplasmonic effects induced by plasmonic absorbers have enabled the investigation of such structures as nanoscale heat sources in many applications. Furthermore by integrating plasmonic absorbers, nanomechanical devices with extremely high mass, force, and displacement sensitivities can achieve unique functionalities such as thermal optomechanical infrared detection [23]–[36].

In a previous publication, we theoretically demonstrated that a nanorod antenna array with an areal coverage of only 2.5% can be an efficient mid-infrared absorber with 10 times larger absorption compared to a uniform metal film of the same thickness [37]. In this letter, we experimentally demonstrate that the localized optical energy in nanoplasmonic resonators can be efficiently converted to mechanical energy and actuate nanomechanical structures for infrared (IR) thermal detector applications. A schematic of the plasmomechanical device with optical readout is shown in Fig. 1. A gold nanorod antenna absorber fabricated on a silicon nitride membrane, a well-known mechanical resonator platform [38], [39], forms the central part of the device. The resonant wavelength of the plasmonic antenna absorber is tuned to 6 μm. On resonance, the plasmonic antenna absorber efficiently converts the incoming infrared radiation into thermal energy. Due to the mismatch between the thermal expansion coefficients of the silicon nitride membrane and gold nanorods, the increased temperature caused by IR absorption, in turn, drives the membrane to mechanically deflect. The mechanical deflection of the membrane is then read out optically by a fiber-optic interferometer based on a Fabry–Perot cavity formed by the backside of the membrane and the end face of a bare fiber [40]. The total reflectivity of the interferometer is highly sensitive to the distance between the two reflectors [41]. Light from a 1550 nm laser is coupled into the interferometer through a fiber-optic circulator and the reflected optical power is converted into signal current by a photodetector. The final output current I_{OUT} from the detector is related to the input IR power P_{IR} by:

$$I_{\mathrm{OUT}} = P_{\mathrm{IR}} \times \eta_{\mathrm{ant}} \times \eta_{\mathrm{T/P}} \times \eta_{\mathrm{Z/T}} \times \eta_{\mathrm{FP}} \times \eta_{\mathrm{PD}}. \tag{1}$$

Here, η_{ant} is the absorption efficiency of the plasmonic antenna absorber, $\eta_{\mathrm{T/P}}$ is the rate of temperature increase per unit absorbed power, and $\eta_{\mathrm{Z/T}}$ is the mechanical deflection per unit temperature increase in units of nm/K. $\Delta z = P_{\mathrm{IR}} \times \eta_{\mathrm{ant}} \times \eta_{\mathrm{T/P}} \times \eta_{\mathrm{Z/T}}$ is the mechanical deflection of the membrane caused by the absorbed IR power. $\eta_{\mathrm{FP}} = dP_{\mathrm{FPr}}/dz$ is defined as the power sensitivity of the fiber-optic interferometer. η_{PD} is the quantum efficiency of the photodetector. The current responsivity of the plasmomechanical infrared detector is defined as $R_{\mathrm{IR}} = I_{\mathrm{OUT}}/P_{\mathrm{IR}}$.

Manuscript received October 8, 2013; revised November 6, 2013; accepted November 12, 2013. Date of publication December 5, 2013; date of current version December 31, 2013.

The authors are with the Department of Material Science and Engineering, University of Pennsylvania, Philadelphia, PA 19104 USA (e-mail: cubukcu@seas.upenn.edu).

Color versions of one or more of the figures in this letter are available online at http://ieeexplore.ieee.org.

Digital Object Identifier 10.1109/LPT.2013.2292307

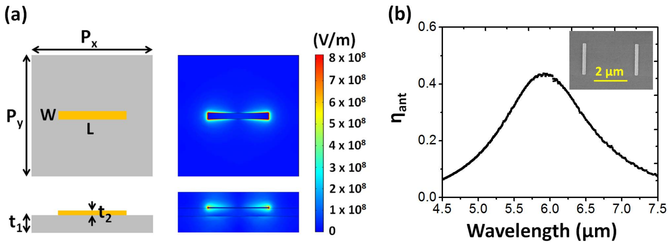

Fig. 2. (Color online) (a) The schematic structure of the unit cell and the distribution of electric field norm |E| in the near field of the nanorod antenna. (b) The typical measured optical absorption spectrum of the nanoantenna absorber, using Fourier Transform Infrared Spectroscopy (FTIR). The inset shows the scanning electron microscopy image of the nanorod antennas fabricated on silicon nitride with $W = 200$ nm, $L = 1850$ nm, $P_x = P_y = 3000$ nm and $t_1 = 100$ nm and $t_2 = 25$ nm (5 nm of Ti and 20 nm of Au).

II. Plasmonic Nanoantenna Absorber

In order to determine the absorption coefficient η_{ant} of the plasmonic antenna absorber, we first studied the resonant property of the plasmonic antenna absorber on a silicon nitride membrane using a finite element method [42]. The simulated structure is a unit cell of the periodic structure as shown in Fig. 2. The unit cell includes a gold nanorod on the membrane. p_x and p_y are the periods of the gold nanorod array in the x and y directions, respectively. W and L are the width and length of the gold nanorod. t_1 and t_2 are the thicknesses of the gold and the silicon nitride layers. The four sides of the unit cell are set to periodic boundaries. The plane wave excitation of the structure and the detection of the transmitted and reflected power are realized by two user defined ports on the top and bottom of the unit cell. The excitation plane wave is polarized along the length of the rod (E component in the x direction). The localized optical field distribution near gold nanorods is shown in Fig. 2(a). Following our previous theoretical study on nanorod antenna absorbers [37], a peak absorption η_{ant} of about 48% can be obtained at $\lambda = 6$ μm by tuning the geometric parameters such as the width, length and thickness of the gold nanorods.

The inset of Fig. 2(b) shows a nanorod antenna, whose parameters were optimized from numerical simulations, fabricated on a 100 nm thick silicon nitride membrane using electron beam lithography and metal lift-off techniques. We characterized the nanorod absorber arrays by using a Fourier Transform Infrared (FTIR) microscope to verify that the optical resonance is at $\lambda = 6$ μm, as shown in Fig. 2(b).

III. Thermo-Mechanical Actuation

Having determined the absorption coefficient of the plasmonic absorber, we then focus on the thermal actuation of the bilayer structure. Thermo-mechanically driven bilayer cantilever structures have been used as highly sensitive thermal detectors [43]. In our device, the nanorod antennas and the silicon nitride membrane form a bilayer structure which will deflect under increased temperature. The temperature increase caused by the nanorod antenna induced photothermal effect at resonance is first studied numerically using a finite element method code (the heat transfer module of COMSOL 4.2a).

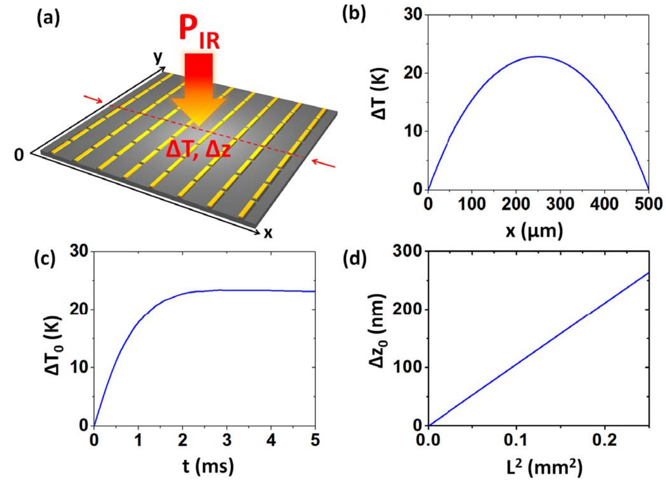

Fig. 3. (Color online) The thermal and mechanical simulation result of the nitride membrane - gold nanorod array bilayer structure with side length L = 500 μm, assuming uniform heat source. (a) The schematic structure of the thermally actuated bilayer membrane. (b) The steady state temperature distribution along the center cut line (y = $L/2$ in (a)) of the bilayer membrane. (c) The temperature increase at the center point of the bilayer structure in the time domain. (d) The linear relationship between the mechanical deflection at the center point of the bilayer structure Δz and the area of the membrane L^2.

The initial temperature of the membrane is set to be 300K and the four edges are assumed to be perfect heat sinks. The total thermal power absorbed by the membrane is set to 1mW. Bulk material properties of the silicon nitride and the gold used in the simulation are from [31]. Fig. 3(b) shows the distribution of the steady state temperature increase ΔT along the center cut line of the membrane under uniform heating. We also compared the numerical simulation result from COMSOL with the analytical solution of the heat transfer equation obtained by the Green's function method and found perfect agreement [31]. The temperature increase at the center point of the bilayer structure in the time domain is also shown in Fig. 3(c). The mechanical deflection of the heated bilayer structure is studied by coupling the heat transfer module with the structural mechanics module of COMSOL. The four edges of the membrane are set to be fixed constraints and we monitored the thermomechanical deflection at the center of the bilayer membrane. From Fig. 3(d), we can see that there is a linear relationship between the mechanical deflection at the center of the membrane Δz and the area of the membrane L^2. At the center point of a membrane with side length $L = 500$ μm ($L^2 = 0.25$ mm^2) under 1 mW of uniform heat source, the calculated mechanical deflection is $\Delta z = 264$ nm.

IV. Measurement of Infrared Response

We next experimentally characterize the thermomechanical response of fabricated membrane devices integrated with the nanorod absorber shown in Fig. 2(b). The detector is put in a vacuum chamber pumped down to $\sim 1\times\ 10^{-5}$ mbar. Fig. 4(a) shows the typical normalized frequency response of the detectors, measured using a sinusoidally modulated 405 nm laser as the excitation. We note that the nanoantenna absorption is not resonant at 405 nm, however, gold is

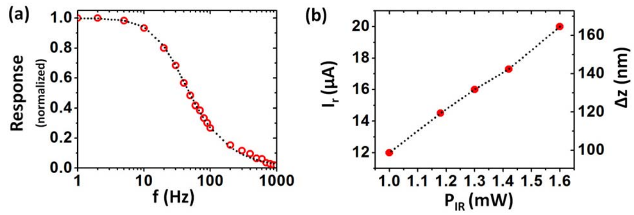

Fig. 4. (Color online) (a) The measured normalized frequency response of the infrared detector. (b) The output current as a function of the input infrared power and the corresponding displacement of the membrane.

absorbing due to bulk interband absorption. The 3 dB cutoff frequency $f_{3\mathrm{dB}}$ is found to be 28 Hz. The time constant τ is therefore $\tau = 1/(2\pi f_{3\mathrm{dB}}) = 5.7$ ms. The discrepancy between the measured time constant and the theoretical value of 1.3 ms indicates that the thermal conductivity of the silicon nitride membrane is lower than the bulk material values used in the simulation [44]. To measure the responsivity of the infrared detector, the output beam of a 6 μm wavelength quantum cascade laser (Daylight Solutions) was used to actuate the membrane. The output beam is modulated by an optical chopper at 10 Hz. The spot size of the beam focused on the membrane by a lens with a focal length of 50 mm is estimated to be around 100 μm. The readout signal from the fiber interferometer is sent to a lock-in amplifier. The operation frequency of the optical chopper is synchronized with the lock-in amplifier. Fig. 4(b) shows that there is a linear relationship between the output current of the photodetector and the input IR power P_{IR}, in agreement with the theoretical prediction. From the curve in Fig. 4(b), the experimentally measured current responsivity is found to be 12 mA/W. The corresponding displacement responsivity is calculated to be 98.7 μm/W. The theoretical current responsivity can be calculated from Eq (1): $R_{\mathrm{IR}} = \eta_{\mathrm{ant}} \times \eta_{\mathrm{Z/P}} \times \eta_{\mathrm{FP\text{-}I}} \times \eta_{\mathrm{lock\text{-}in}} = 0.45 \times 264$ nm/mW $\times\ 0.27\ \mu$A/nm $\times\ 0.45 = 14.4$ mA/W. Here $\eta_{Z/P} \equiv \eta_{T/P} \times \eta_{\mathrm{Z/T}} = 264$ nm/mW is the theoretically calculated mechanical displacement per unit absorbed power (see Section III). $\eta_{\mathrm{FP\text{-}I}} \equiv \eta_{\mathrm{FP}} \times \eta_{\mathrm{PD}} = 0.27\ \mu$A/nm is the current sensitivity of the fiber interferometer. $\eta_{\mathrm{lock\text{-}in}} = 0.45$ is a correction factor for using a lock-in amplifier to measure a square wave generated by the chopper [31]. It can be seen that the theoretical current responsivity is in good agreement with the measured value.

V. Noise Performance

To analyze the noise performance of our device, we consider the fundamental noises from two parts: noises from the membrane, defined as $\overline{p}_{\mathrm{membrane}}$ and noises from the optical readout system, defined as $\overline{p}_{\mathrm{readout}}$. The total noise of the detector $\vec{p}_{\mathrm{total}}$ is then given by:

$$\overline{p}_{\mathrm{total}} = (\overline{p}_{\mathrm{membrane}^2} + \overline{p}_{\mathrm{readout}^2})^{1/2} \tag{2}$$

The noises from the membrane $\overline{p}_{\mathrm{membrane}}$ include the thermal fluctuation noise, the background fluctuation noise, and the thermomechanical vibration noise [33], [34]. The thermal fluctuation noise, defined as $\overline{p}_{\mathrm{th}}$, accounts for the random fluctuations in temperature due to the statistical nature of the heat exchange between the bilayer beam and the supporting silicon frame [34], [35]:

$$\overline{p}_{\mathrm{th}} = (4k_B T^2 G)^{1/2} \tag{3}$$

Here, k_{B} is the Boltzmann constant and $T = 300$ K is the ambient temperature. Under uniform heating, the effective thermal conductance of the membrane structure $G = 4.35 \times 10^{-5}$ W/K was determined from the solution of the heat transfer equation leading to $\overline{p}_{\mathrm{th}} = 14.7$ pW/Hz$^{1/2}$. The background fluctuation noise, defined as $\overline{p}_{\mathrm{RAD}}$, accounts for the random fluctuations in temperature due to the heat exchange between the bilayer beam and the environment through radiation:

$$\overline{p}_{\mathrm{RAD}} = (16A\varepsilon\sigma k T^5)^{1/2} \tag{4}$$

where A is the area of the membrane structure, ε is the emissivity (which is assumed to be 1), and σ is the Stefan–Boltzmann constant. $\overline{p}_{\mathrm{RAD}}$ is found to be 2.8 pW/Hz$^{-1/2}$. Having determined the values of $\overline{p}_{\mathrm{th}}$ and $\overline{p}_{\mathrm{RAD}}$, the noises from the membrane $\overline{p}_{\mathrm{membrane}}$ can be calculated as:

$$\overline{p}_{\mathrm{membrane}} = (\overline{p}_{\mathrm{th}}^2 + \overline{p}_{\mathrm{RAD}}^2)^{1/2}/\eta_{\mathrm{ant}} \tag{5}$$

The off-resonance vibration noise of the bilayer thin film beam arising from $k_{\mathrm{B}T}$ thermal energy can be calculated as:

$$\overline{z}_{\mathrm{vib}} = (4k_{\mathrm{B}}T/\omega_0 kQ)^{1/2} = (4k_{\mathrm{B}}T/\omega_0^3 mQ)^{1/2} \tag{6}$$

where $k = \mathrm{m}\omega_0^2$ is the spring constant, m is the effective mass of the beam, ω_0 is the resonant angular frequency of the beam, and Q is the quality factor of the resonance. Since the measured mechanical resonance frequency f_0 of the first order mode is 250 kHz and the quality factor Q ~7400, the off resonance thermomechanical vibration noise at T = 300K is calculated to be 0.1 fm/Hz$^{1/2}$. The corresponding noise in terms of equivalent input IR power is $\overline{p}_{\mathrm{vib}} = \overline{z}_{\mathrm{vib}}/\eta_{\mathrm{Z/P}} = 0.1$ fm/Hz$^{1/2}$/2.64 $\times\ 10^{-4}$ m/W $= 0.38$ pW/Hz$^{1/2}$. By plugging in the values for the noises calculated above and the measured absorption of the nanoantenna $\eta_{\mathrm{ant}} = 0.4$, $\overline{p}_{\mathrm{membrane}}$ is calculated to be about 37.4 pW/Hz$^{1/2}$.

The noises from the optical readout part $\overline{p}_{\mathrm{readout}}$ include the shot noise of the photodetector, the relative intensity noise (RIN) of the 1550 nm laser, and the noise from the current-to-voltage converter. Following the same procedure in our previous work on thermo-mechanical infrared detectors, the readout noise equivalent power at the low frequency limit is calculated to be $\overline{p}_{\mathrm{readout}} = 358$ pW/Hz$^{1/2}$ [31]. The total noise of the detector $\overline{p}_{\mathrm{total}}$ is then determined to be 359 pW/Hz$^{1/2}$. Therefore our device is limited by the noises from the readout part. For the $1/f$ noise and other noises in the low frequency range, please see the supporting information for details.

VI. Conclusion

We have experimentally demonstrated a membrane based thermal infrared detector with an integrated plasmonic absorber. Efficient conversion from optical energy to mechanical energy is achieved by thermo-mechanical actuation of a membrane through the dissipated optical energy in the plasmonic resonances. With an integrated fiber-optic interferometric readout, a thermal infrared detection responsivity of 12 mA/W (displacement responsivity is 98.7 μm/W) and a time constant of 5.7 ms are demonstrated at $\lambda = 6$ μm. The working wavelength can be tuned to the near infrared or terahertz region by modifying the dimensions of the nanoantenna. This approach enables any mechanical resonator to be optically responsive for photothermal actuation, which will be advantageous in hybrid optomechanical infrared sensors and devices.

References

[1] S. A. Maier and H. A. Atwater, "Plasmonics: Localization and guiding of electromagnetic energy in metal/dielectric structures," *J. Appl. Phys.*, vol. 98, no. 1, pp. 011101-1–011101-10, Jul. 2005.

[2] A. V. Zayats, I. I. Smolyaninov, and A. A. Maradudin, "Nano-optics of surface plasmon polaritons," *Phys. Rep.*, vol. 408, nos. 3–4, pp. 131–314, Mar. 2005.

[3] A. L. Lereu, "Modulation—Plasmons lend a helping hand," *Nature Photon.*, vol. 1, pp. 368–369, Jul. 2007.

[4] A. Passian, A. L. Lereu, E. T. Arakawa, A. Wig, T. Thundat, and T. L. Ferrell, "Modulation of multiple photon energies by use of surface plasmons," *Opt. Lett.*, vol. 30, no. 1, pp. 41–43, Jan. 2005.

[5] B. Rothenhausler and W. Knoll, "Surface–plasmon microscopy," *Nature*, vol. 332, pp. 615–617, Apr. 1988.

[6] A. N. Grigorenko, P. I. Nikitin, and A. V. Kabashin, "Phase jumps and interferometric surface plasmon resonance imaging," *Appl. Phys. Lett.*, vol. 75, no. 25, pp. 3917–3919, Dec. 1999.

[7] S. M. Nie and S. R. Emery, "Probing single molecules and single nanoparticles by surface-enhanced Raman scattering," *Science*, vol. 275, no. 5303, pp. 1102–1106, Feb. 1997.

[8] M. E. Mezeme and C. Brosseau, "Engineering nanostructures with enhanced thermoplasmonic properties for biosensing and selective targeting applications," *Phys. Rev. E*, vol. 87, no. 1, pp. 012722-1–012722-10, Jan. 2013.

[9] A. O. Govorov and H. H. Richardson, "Generating heat with metal nanoparticles," *Nano Today*, vol. 2, no. 1, pp. 30–38, Feb. 2007.

[10] H. H. Richardson, Z. N. Hickman, A. O. Govorov, A. C. Thomas, W. Zhang, and M. E. Kordesch, "Thermooptical properties of gold nanoparticles embedded in ice: Characterization of heat generation and melting," *Nano Lett.*, vol. 6, no. 4, pp. 783–788, Apr. 2006.

[11] X. Huang, I. H. El-Sayed, W. Qian, and M. A. El-Sayed, "Cancer cell imaging and photothermal therapy in the near-infrared region by using gold nanorods," *J. Amer. Chem. Soc.*, vol. 128, no. 6, pp. 2115–2120, Feb. 2006.

[12] A. M. Gobin, D. P. O'Neal, D. M. Watkins, N. J. Halas, R. A. Drezek, and J. L. West, "Near infrared laser-tissue welding using nanoshells as an exogenous absorber," *Lasers Surgery Med.*, vol. 37, no. 2, pp. 123–129, Aug. 2005.

[13] P. K. Jain, K. S. Lee, I. H. El-Sayed, and M. A. El-Sayed, "Calculated absorption and scattering properties of gold nanoparticles of different size, shape, and composition: Applications in biological imaging and biomedicine," *J. Phys. Chem. B*, vol. 110, no. 14, pp. 7238–7248, Apr. 2006.

[14] G. Baffou, R. Quidant, and C. Girard, "Heat generation in plasmonic nanostructures: Influence of morphology," *Appl. Phys. Lett.*, vol. 94, no. 15, pp. 153109-1–153109-3, Apr. 2009.

[15] G. Baffou, R. Quidant, and F. Javier García de Abajo, "Nanoscale control of optical heating in complex plasmonic systems," *ACS Nano*, vol. 4, no. 2, pp. 709–716, Feb. 2010.

[16] K. Aydin, V. E. Ferry, R. M. Briggs, and H. A. Atwater, "Broadband polarization-independent resonant light absorption using ultrathin plasmonic super absorbers," *Nature Commun.*, vol. 2, p. 517, Nov. 2011.

[17] C. Wu, B. Neuner, and G. Shvets, "Large-area wide-angle spectrally selective plasmonic absorber," *Phys. Rev. B*, vol. 84, no. 7, pp. 075102-1–075102-7, Aug. 2011.

[18] H. Tao, *et al.*, "A dual band terahertz metamaterial absorber," *J. Phys. D, Appl. Phys.*, vol. 43, no. 22, pp. 225102–225106, Jun. 2010.

[19] A. Passian, A. L. Lereu, R. H. Ritchie, F. Meriaudeau, T. Thundat, and T. L. Ferrell, "Surface plasmon assisted thermal coupling of multiple photon energies," *Thin Solid Films*, vol. 497, nos. 1–2, pp. 315–320, Feb. 2006.

[20] A. L. Lereu, A. Passian, R. H. Farahi, N. F. van Hulst, T. L. Ferrell, and T. Thundat, "Thermoplasmonic shift and dispersion in thin metal films," *J. Vac. Sci. Technol. A, Vac., Surf., Films*, vol. 26, no. 4, pp. 836–841, Jul. 2008.

[21] A. L. Lereu, R. H. Farahi, L. Tetard, S. Enoch, T. Thundat, and A. Passian, "Plasmon assisted thermal modulation in nanoparticles," *Opt. Express*, vol. 21,no. 10, pp. 12145–12158, May 2013.

[22] A. L. Lereu, A. Passian, R. H. Farahi, L. Abel-Tiberini, L. Tetard, and T. Thundat, "Spectroscopy and imaging of arrays of nanorods toward nanopolarimetry," *Nanotechnology*, vol. 23, no. 4, p. 045701, Feb. 2012.

[23] X. Sun, J. Zheng, M. Poot, C. W. Wong, and H. X. Tang, "Femtogram doubly clamped nanomechanical resonators embedded in a high-Q two-dimensional photonic crystal nanocavity," *Nano Lett.*, vol. 12, no. 5, pp. 2299–2305, May 2012.

[24] A. K. Naik, M. S. Hanay, W. K. Hiebert, X. L. Feng, and M. L. Roukes, "Towards single-molecule nanomechanical mass spectrometry," *Nature Nanotechnol.*, vol. 4, pp. 445–450, Jul. 2009.

[25] Y. T. Yang, C. Callegari, X. L. Feng, K. L. Ekinci, and M. L. Roukes, "Zeptogram-scale nanomechanical mass sensing," *Nano Lett.*, vol. 6, no. 4, pp. 583–586, Apr. 2006.

[26] K. Jensen, K. Kim, and A. Zettl, "An atomic-resolution nanomechanical mass sensor," *Nature Nanotechnol.*, vol. 3, pp. 533–537, Sep. 2008.

[27] J. D. Teufel, T. Donner, M. A. Castellanos-Beltran, J. W. Harlow, and K. W. Lehnert, "Nanomechanical motion measured with an imprecision below that at the standard quantum limit," *Nature Nanotechnol.*, vol. 4, pp. 820–823, Dec. 2009.

[28] M. D. LaHaye, O. Buu, B. Camarota, and K. C. Schwab, "Approaching the quantum limit of a nanomechanical resonator," *Science*, vol. 304, no. 5667, pp. 74–77, Apr. 2004.

[29] R. G. Knobel and A. N. Cleland, "Nanometre-scale displacement sensing using a single electron transistor," *Nature*, vol. 424, pp. 291–293, Jul. 2003.

[30] P. G. Datskos, N. V. Lavrik, and S. Rajic, "Performance of uncooled microcantilever thermal detectors," *Rev. Sci. Instrum.*, vol. 75, no. 4, pp. 1134–1148, Apr. 2004.

[31] F. Yi, H. Zhu, J. C. Reed, and E. Cubukcu, "Plasmonically enhanced thermomechanical detection of infrared radiation," *Nano Lett.*, vol. 13, no. 4, pp. 1638–1643, Mar. 2013.

[32] H. Tao, *et al.*, "Microwave and terahertz wave sensing with metamaterials," *Opt. Express*, vol. 19, no. 22, pp. 21620–21626, Oct. 2011.

[33] T. W. Kenny, W. J. Kaiser, S. B. Waltman, and J. K. Reynolds, "Novel infrared detector based on a tunneling displacement transducer," *Appl. Phys. Lett.*, vol. 59, no. 15, pp. 1820–1822, Oct. 1991.

[34] Y. Zhao, *et al.*, "Optomechanical uncooled infrared imaging system: Design, microfabrication, and performance," *J. Microelectromech. Syst.*, vol. 11, no. 2, pp. 136–146, Apr. 2002.

[35] P. W. Kruse and D. D. Skatrud, *Uncooled Infrared Imaging Arrays and Systems*. San Diego, CA, USA: Academic, 1997.

[36] F. Alves, D. Grbovic, B. Kearney, and G. Karunasiri, "Microelectromechanical systems bimaterial terahertz sensor with integrated metamaterial absorber," *Opt. Lett.*, vol. 37, no. 11, pp. 1886–1888, Jun. 2012.

[37] H. Zhu, F. Yi, and E. Cubukcu, "Nanoantenna absorbers for thermal detectors," *IEEE Photon. Technol. Lett.*, vol. 24, no. 14, pp. 1194–1196, Jul. 15, 2012.

[38] B. M. Zwickl, *et al.*, "High quality mechanical and optical properties of commercial silicon nitride membranes," *Appl. Phys. Lett.*, vol. 92, no. 10, pp. 103125-1–103125-3, Mar. 2008.

[39] P.-L. Yu, T. P. Purdy, and C. A. Regal, "Control of material damping in high-Q membrane microresonators," *Phys. Rev. Lett.*, vol. 108, no. 8, pp. 083603-1–083603-5, Feb. 2012.

[40] O. Kilic, M. Digonnet, G. Kino, and O. Solgaard, "External fibre Fabry–Pérot acoustic sensor based on a photonic-crystal mirror," *Meas. Sci. Technol.*, vol. 18, no. 10, pp. 3049–3054, Oct. 2007.

[41] H. I. Rasool, P. R. Wilkinson, A. Z. Stieg, and J. K. Gimzewski, "A low noise all-fiber interferometer for high resolution frequency modulated atomic force microscopy imaging in liquids," *Rev. Sci. Instrum.*, vol. 81, no. 2, pp. 023703-1–023703-10, Feb. 2010.

[42] *COMSOL Multiphysics 4.2a*, COMSOL Inc., Burlington, MA, USA, 2011.

[43] J. Lai, T. Perazzo, Z. Shi, and A. Majumdar, "Optimization and performance of high-resolution micro-optomechanical thermal sensors," *Sens. Actuators A, Phys.*, vol. 58, no. 2, pp. 113–119, Feb. 1997.

[44] G. Chen, *Nanoscale Energy Transport and Conversion*. New York, NY, USA: Oxford Univ. Press, 2005.